Mengoli, G., et al., *Anomalous heat effects correlated with electrochemical hydriding of nickel.* Nuovo Cimento Soc. Ital. Fis. A, 1998. **20 D**: p. 331

Anomalous heat effects correlated with electrochemical hydriding of nickel

G. MENGOLI (1), M. BERNARDINI (1), C. MANDUCHI (2) and G. ZANNONI (2)
(1) *CNR IPELP - Corso Stati Uniti 4. 35127 Padova, Italy*
(2) *Dipartimento di Fisica, University di Padova - via Marzolo 8, 35131 Padova, Italy*

(ricevuto I'll Luglio 1996; revisionato it 29 Novembre 1996; approvato it 23 Settembre 1997)

Summary. — The hydrogen evolution reaction at sintered nickel in H_2O-K_2CO_3 electrolyte was investigated by electrochemical and calorimetric techniques. Hydrogen evolution was accomplished with surface conversion of Ni into β-Ni-hydride, the extent of this reaction being strongly enhanced by temperature. Isoperibolic or isothermal calorimetry measurements show that electrochemical hydriding, especially at a temperature close to the boiling point of the electrolyte, is paralleled by anomalous heat evolution in large excess of electric power input. Electrochemically activated Ni electrodes, led in open circuit, keep on doing heat.

PACS 65.90 — Other topics in thermal properties of condensed matter.

1. – Introduction

Although generation of excess energy by electrolytic reduction of light water at either nickel or other metal cathodes was claimed by Fleischmann and Pons in their 1989 patent [1] it was subsequently not verified.

The first detailed study on the subject was that published two years later by Mills and Kneizys [2]. They found a power output several times exceeding the Joule power input during electrolysis with low current density of aqueous K_2CO_3 at Ni plate electrodes: no anomalous effects were observed with Na_2CO_3 electrolyte.

According to Mills, exotic physics were involved, whereby hydrogen atoms shrink, releasing energy, to levels below the ground state: this transition requires an electrocatalytic mechanism working with potassium but energetically forbidden with sodium.

Noninsky, was the first to confirm Mills' findings through reliable heat loss differential calorimetry [3].

In 1992, Bush published new data on the H_2O-Ni system [4]. Excess heat was systematically observed, even in experiments with Na_2CO_3, when carbonates of various alkaline metals were used. The "shrunken" hydrogen model was consequently rejected and "alkali-hydrogen fusion"

suggested, whereby alkaline metals are transmuted into elements of higher nuclear stability ("magic number" nuclei).

At the ICCF IV meeting, Srinivasan *et al.* [5] independently reported both excess heat and tritium generation during electrolytic reduction of aqueous alkali solutions at the Ni cathode.

In 1993, two works were published on the subject. The first, by Notoya [6] gave solid evidence of the thermal phenomenon: not only was the power output three times higher than the power input, but this level was attained in a few hours, so that calorimetric measurements were probably not affected by the errors and/or artifacts which may occur during long electrolyses. The above author used a small ($1.0 \times 0.5 \times 0.1$ cm^3) sintered Ni cathode which sustained high current (0.5 A) with remarkable specific power production (1 W/cm^2). Results were interpreted according to Bush's hypothesis.

The second work, by Ohmori and Enyo [7], investigated other electrolytes (alkaline sulfates and carbonates) and metal cathodes (Ag, Au, Sn) in addition to the H_2O/K_2CO_3-Ni system: anomalous heat effects were observed in most of the systems excluding H_2O/Na_2 CO_3-Ni and H_2O/Li_2 SO_4-Ni.

In 1994 Mills *et al.* [8] and Mills and Good (1995) [9] again published works on the calorimetry of H_2O reduction at Ni. Having increased the scale of the original process, greater excess power (41 W, eight times the $I \times V$ total input power) was measured with K_2CO_3, whereas negative results were again obtained with Na_2CO_3.

In 1994, Focardi, Piantelli and Habel [10] reported that the interaction of sub-atmospheric H_2 (500-600 mBar) with Ni at temperatures of over 200°C gave rise to large enthalpy release. Hydrogen was loaded into the Ni sample using electromagnetic fields and temperature/pressure perturbations: after a long period of induction the system evolved into a state in which heat (≥3 5 W/cm^2) was emitted and was steadily self-sustaining for months.

The above literature, although not exhaustive, lists the most important contributions to this intriguing topic. It is now possible to draw the following conclusions:

– The evidence of excess heat generation by electrolysis of light water at Ni (or by means of H2-Ni interaction) appears to be sound and self-consistent, having been accomplished by various research groups using different calorimetric techniques.

– Compared with the number of negative papers denying the Fleischmann-Pons effect, very few negative results on the H_2O-Ni system have been reported: the only paper denying the generation of excess heat is probably that published by Shkedi *et al.* in 1995 [11]. Although these authors did observe some heat exceeding electrolytic Joule power, it was considered to be an artifact, due to low faradaic efficiency and underestimation of the true Joule power input.

– The origin of enthalpy generation is totally unknown: Mills' hypothesis requiring potassium salt electrocatalysis is weakened by the positive results obtained with Na_2CO_3,

whereas the “alkali-hydrogen fusion” is challenged by the Piantelli experiment, in which no alkali metal was involved.

We believe that the findings of both Mills and Piantelli have a common origin: in other words, that the thermal effects observed in either electrolytic or dry environments start from the same physical-chemical state of the system. Although this is far from being an explanation of the phenomenon, but elucidation of the physicochemical conditions suitable for its induction is the first step towards understanding it.

The present investigation was undertaken to reveal the relation, if any, between cathodic activation of Ni and heat generation.

2. – Experimental

2.1. Materials

– Sintered Ni sheet 0.06 cm thick (density ≈ 6 gcm^{-3}), supplied by Wiggin Alloys Limited (GB) under the trade name Kelac 47;

– Ni sheet (0.02 cm thick) and Ni rod (Φ = 1.0 cm) 99.9% purity, supplied by Goodfellow (GB);

– Ni wire (Φ = 0.1 cm) 99.5 purity, from Carlo Erba (Milan);

– Pt wire (Φ = 0.1 cm) 99.9 purity, from Metalli Preziosi (Milan);

– K_2CO_3, Na_2CO_3, and other chemicals were reagent grade from Carlo Erba;

– H_2O: “Millipore” grade;

– N_2 was high-purity gas from S.I.O. (Padova);

– Cells and glass components were made of Pyrex.

2.2. Apparatus

a) Electrochemical runs. The electrochemical apparatus was assembled with AMEL units (553 potentiostat; 566 function generator; 731 integrator).

The electrolytic cell was a double-jacketed glass cylinder, thermostated with a mantle of silicon oil by a Haake F3 thermostat. The lid of the cell supported the electrodes and connected the electric cables to the apparatus. The working electrode, aced in the middle of the lid, was composed of a Ni plate (sintered or massive Ni) pressure-bonded to a Ni wire serving as the electric connection. A Pt wire coil around e Ni plate was the counter-electrode and a saturated calomel electrode (s.c.e.), separated from the working electrode by a Luggin capillary, was the reference. For work at high temperature (95°C), the reference electrode was an oxidized Ag wire the potential of which was ≈ 50 mV positive with respect to the s.c.e. Basic experiments (potentiostatic electrolysis; cyclic voltammetry; potential steps; coulometry) performed with the

above apparatus concerned study of the hydrogen evolution reaction in alkaline media at Ni and any resulting modifications induced in the metal.

b) Calorimetry. The type of cell adopted for measuring heat effects correlated with water discharge at Ni is shown in fig. 1. It consisted of a Dewar cylinder equipped a refrigerating column to condense and reflux water vaporized from the electrolyte. The body of the cylinder was immersed in a thermostated silicon oil bath, at a stable temperature (accuracy ± 0.01°C) by a Haake F3 thermostat. The column was refrigerated by a controlled stream of tap water.

The internal dimensions of the cell were: $\Phi = 4$ cm, $h = 17$ cm, useful capacity ≈ 110 cm^3. The top seal was a "Teflon" lid supporting the cathode (W), anode (C), thermometer (T), heater (R) and glass pipe bubbler.

Two cells were used: one with air in the hollow space of the Dewar cylinder and a lid 5 cm thick, and one with vacuum in the interspace and a lid 3 cm thick: the latter, which lower sensitivity in the adopted calorimetry, was mainly used for calibration purposes.

The cathode was a Ni strip pressure-bonded to Ni wire; the anode was a cylindrical coil of Ni (or Pt) wire ($l = 130$ cm) surrounding the cathode. Both cathode and anode were externally connected by running the end of the Ni (or Pt) wire through a Pyrex tube sealed with epoxy resin up through the electrolyte and then through the lid.

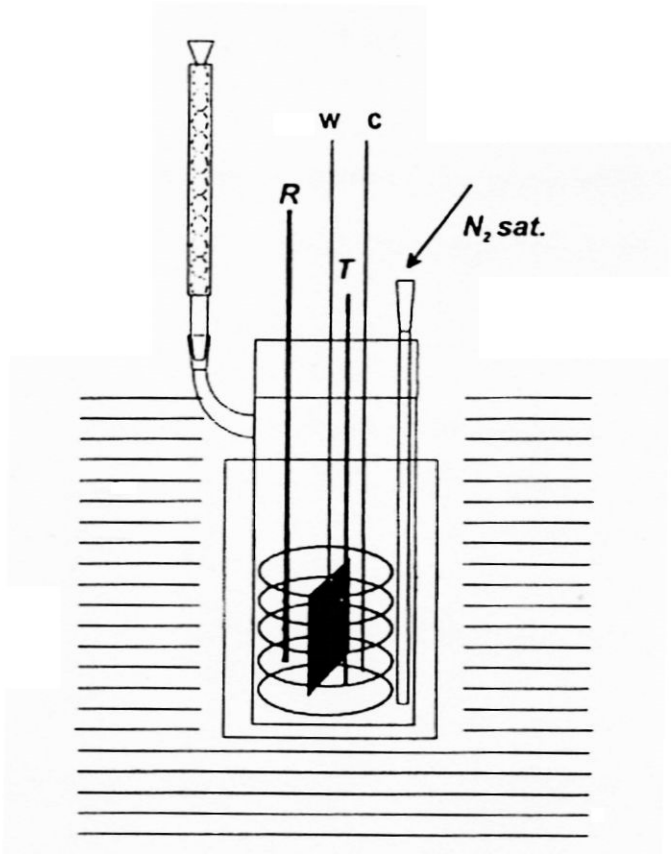

Figure 1. – Dewar electrolytic cell used for calorimetry.

The electrolysis current, stabilized at 1%, was fed by a mod. 553 AMEL galvanostat, the potential difference between cathode and anode being monitored by a Keithley 175 A multimeter.

A Pt 100 thermoresistance sampled by a Wheatstone bridge constituted the thermometric system: all equipment was manufactured by Thermo Engineering, Cremona. Two devices were alternatively used with respective temperature ranges of -40/100°C and 0/200°C. The thermometric system was fed by a high-stability mod. 401 Ortec 24 V power generator to obtain temperature as electric current, monitored continuously by a Keithley 175 A multimeter. Current readings were made at ± 1 μA sensitivity which corresponded to 0.009°C for the first thermometer (-40/100°C) and 0.012°C for the second.

The heater was constructed by coiling a Ni-Cr wire (Φ = 0.03 cm) round a glass mesh support and then forcing it into a thin-walled Pyrex tube sealed at one end: the required resistance was obtained by using Ni-Cr coils of various lengths (90-150 cm). The heater, deeply immersed in the cell so as to have ≈ 5 cm of electrolyte above the resistive element, was fed by a mod 553 AMEL galvanostat, applied voltage being monitored by a Keithley 175 A multimeter.

The glass pipe bubbler conveyed a continuous, controlled stream of gas, generally into the cell, ensuring homogeneous heat distribution within the electrolyte while minimizing the risk of explosive H_2-O_2 recombination (in the gas phase).

The gas line comprised the gas cylinder, manually operated valves (HBS regulators, Padova - L'Air Liquide, Montigny), and a presaturator filled with H_2O in which the gas was saturated with moisture before being bubbled into the electrolyte. The gas left the cell through the refrigerating column and reached an external bubbler containing paraffin, to insulate the system from the atmosphere.

The valve-adjusted gas flow was measured by counting the bubbles flowing through the presaturator in one min, this rate being standardized in ml/min by a flowmeter.

3. – Results

3.1. Electrochemical runs

a) Electrode behavior of sintered Ni. The sintered Ni electrode, dipped in 0.6 M K_2CO_3/H_2O electrolyte, acquired an open circuit (o.c.) potential in the range -0.2/ -0.5 V *vs.* s.c.e., the more negative potential being typical of prolonged immersion and probably reflecting adsorption of hydroxyl ions and $Ni(OH)_2$ formation. When the electrode potential was shifted in the anodic direction, the Ni surface was converted into insoluble oxides on which H_2O was eventually oxidized to O_2 and protons: this is the process sustained by the anode during electrolysis.

However, the reactions which concern this work were those which occurred when Ni was polarized negative with respect to its o.c. potential. These reactions were investigated by means of several diagnostic electrochemical techniques.

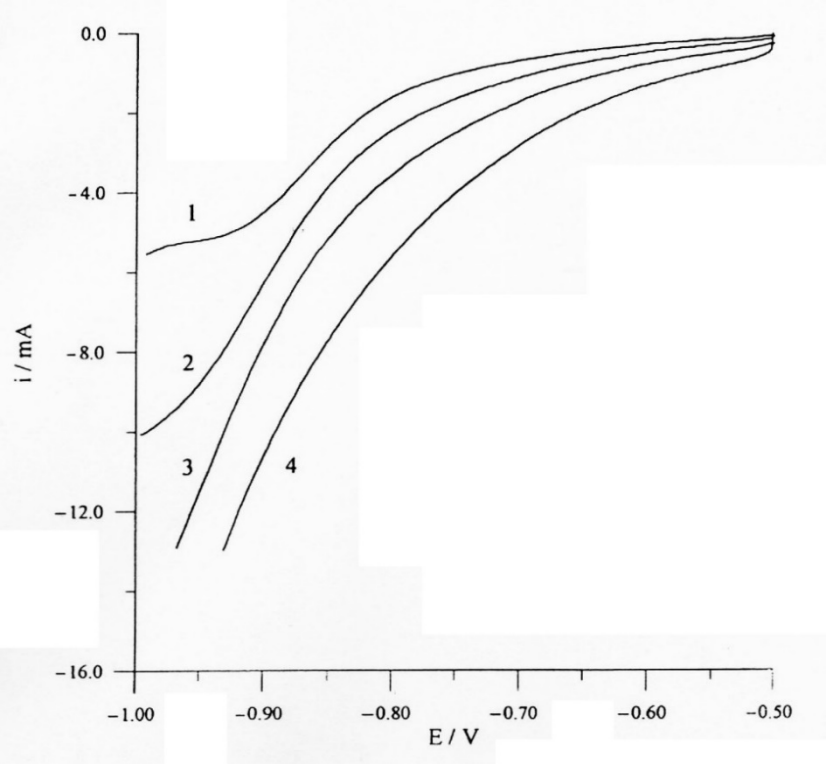

Figure 2. – Linear sweep voltammetry of 0.6 M K_2CO_3 reduction at sintered Ni (area ≈ 3.3 cm^2). Sweep rates: 1) 5 mV/s; 2) 10 mV/s; 3) 20 mV/s; 4) 50 mV/s.

Figure 2 shows the current response of the Ni electrode at 25°C when cathodically polarized by linear sweep voltammetry: an increasing negative potential was applied to the original potentiostatic polarization at -0.50 V, to reach -1.0 V, using four different potential sweep rates (*v*). The negative currents which are seen to increase with and to outline a limiting current plateau, would indicate a reduction process taking place with a more positive value than the hydrogen evolution reaction.

When, instead of using the potential sweep technique, the Ni electrode was cathodically polarized in steps, by recording the current attained after a given electrolysis time for each step, a steady-state current could not easily be observed, as it decreased with electrolysis time. This behavior is explained in fig. 3, in which the current recorded after 15 s of potentiostatic electrolysis for each step (curve a) is compared with that obtained after 3 min of electrolysis (curve b). The results of fig. 3 may be diagnostic of a process leading to surface formation of a new phase having different electroactivity with respect to the bare Ni surface. In this view, the current plateau of fig. 2 is due to the formation of some Ni-hydride phase by reaction of Ni with underpotential discharged hydrogen.

For a better insight into this process, the Ni electrode was submitted to short cathodic potentiostatic electrolyses and its potential was then stepped some tens of mV more positive. The results of a typical experiment are shown in fig. 4, in which three steps of increasing amplitude were applied to Ni, each after a potentiostatic period (30 s) at -1.0 V. It may be seen that H_2O

reduction was paralleled by the formation of a species which was very easily oxidized (anodic currents were in fact obtained for each step). The oxidation current increased with the amplitude of the potential step: the only species which could be oxidized within the range of H_2O reduction was hydrogen, more properly hydrogen bound to the metal, *i.e.*, NiH_x.

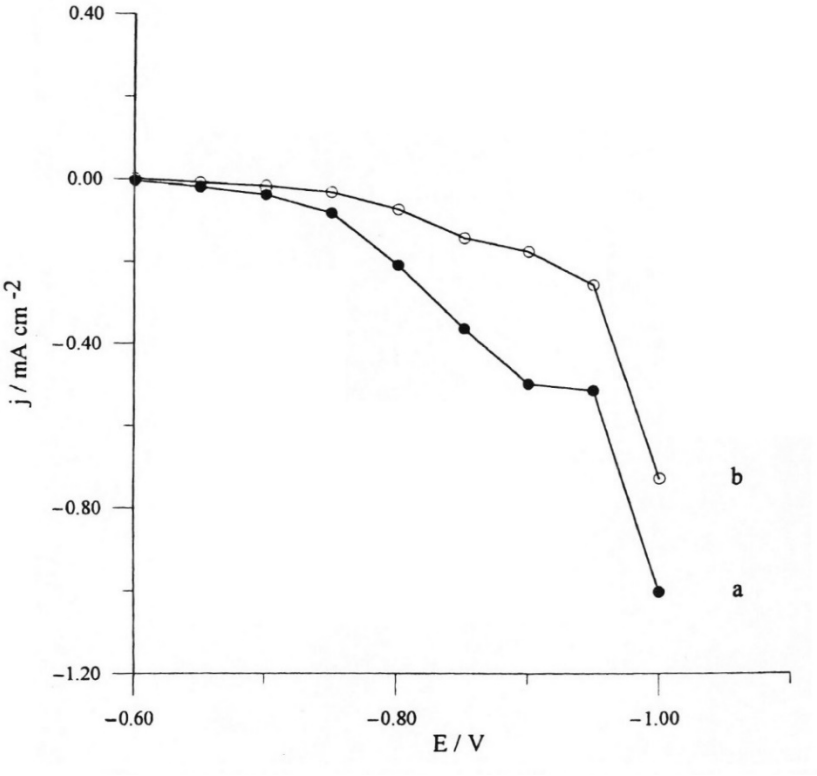

Figure 3. – Cathodic current-potential curves obtained stepwise from system of fig. 2. Length of potentiostatic steps: ●, 15 s; ○, 3 min.

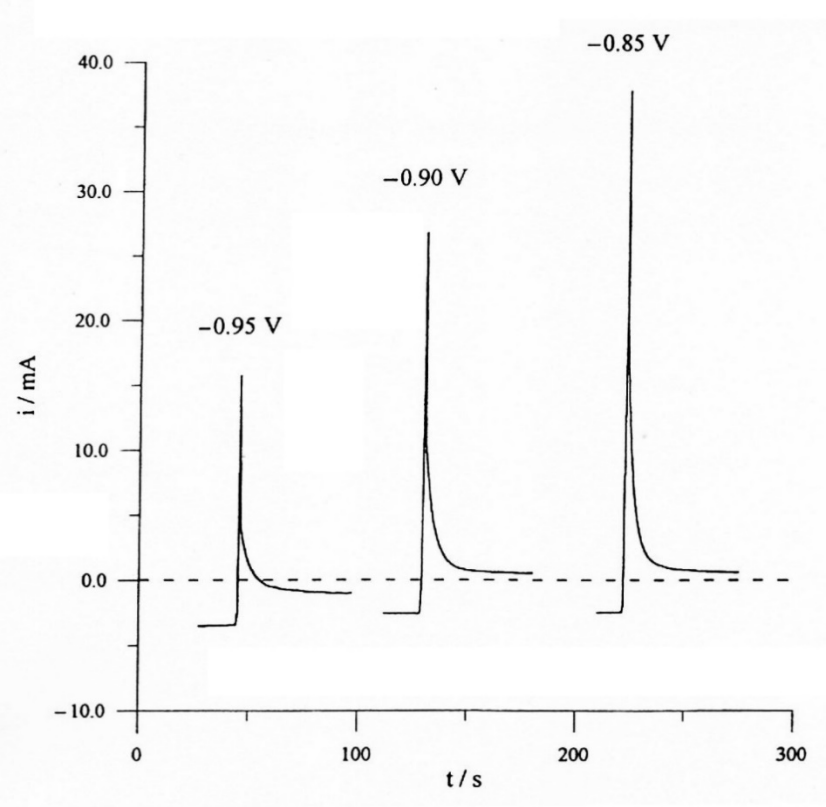

Figure 4. – Anodic current transients obtained from system of fig. 2 by stepping the electrode potential from -1.00 V to less negative values.

The data of fig. 4 may explain the peculiarities of figs. 2 and 3.

The Volmer-Tafel ((1) and (3)) and Volmer-Heyrovsky ((1) and (4)) reactions typical of the hydrogen evolution reaction (h.e.r.) at transition metal electrodes:

(1) $H_2O\ Ni + e \rightarrow NiH_{ads} + {}^{-}OH$,

(2) $NiH_{ads} \rightarrow NiH_{bulk}$,

(3) $2\ NiH_{ads} \rightarrow Ni + H_2$,

(4) $H_2O + NiH_{ads} + e \rightarrow Ni + H_2 + {}^{-}OH$,

are paralleled by the formation of a bulk or subsurface hydride (reaction 2).

The nature of the Ni-hydride phase may be inferred from the experiment reported in fig. 5. Here, after potentiostatic electrolysis at -0.1 V (30 s), the electrode was always polarized in the anodic direction by potential sweep voltammetry: the resulting current-potential curves point to two anodic processes, the former (more negative), probably due to the oxidation of the more energetic hydride species, *i.e.*, β-NiH_x phase, and the latter linked to interstitial hydrogen in the α-NiH_x phase.

The formation of β-Ni-hydride was further confirmed by measuring the o.c. potential acquired by the electrode after potentiostatic electrolysis in the range -1.0/ -1.1 V. Figure 6 shows the o.c. potential decay *vs.* time measured for a Ni electrode previously polarized for 60 min at -1.05 V. The initially recorded o.c. potential is similar to that of a Pd electrode converted into the $PdH_{0.6}$ phase: the subsequent o.c. potential decay is due to the decomposition of NiH_x as a result of its thermodynamic instability [12].

The experiments of figs. 2-6 were performed at room temperature; the same voltammetric behavior was tested at 60°C and 95°C, but hydrogen absorption was seen to increase significantly with temperature. This is shown in table I which reports the hydrogen absorbed as β-hydride phase by the same electrode in various electrolysis conditions (duration of electrolysis and/or electrolysis potential) at three different temperatures. Absorbed hydrogen was measured as the positive charge stripped from the electrode after each cathodic electrolysis. The amount of hydrogen extracted in each run, as well the shape of the extraction current transient, are diagnostic of rather limited penetration of hydrogen into the metal: assuming that the β-hydride has $NiH_{0.8}$ stoichiometry [12] and that the geometric area of the sintered Ni electrode fits its real surface (a rough approximation), it was estimated that the hydriding reaction involves from a few hundred to a few thousand Ni layers.

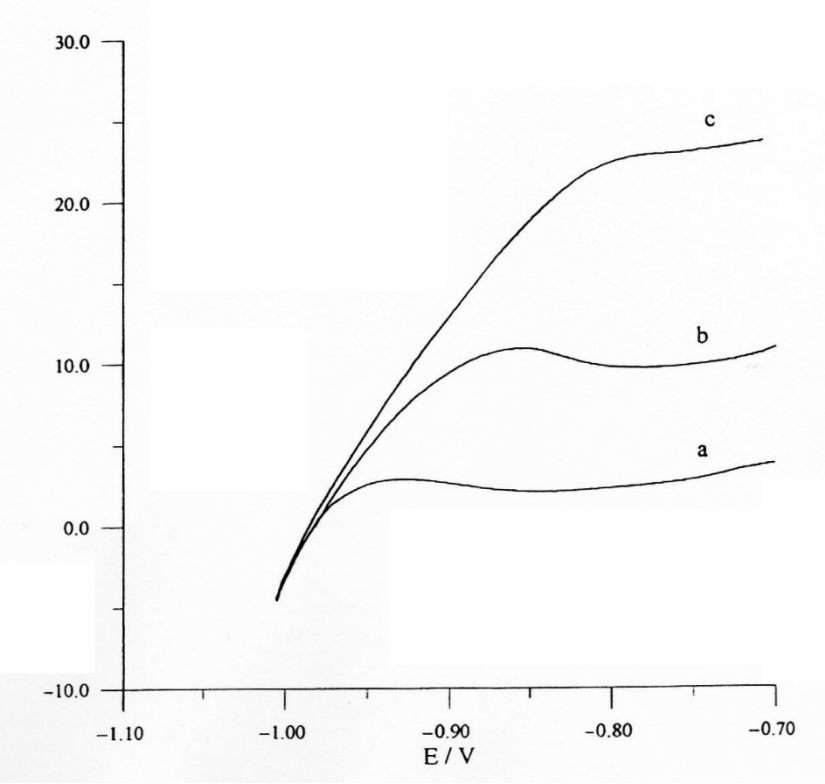

Figure 5. – Anodic voltammetric curves obtained from system of fig. 2 after potentiostatic reduction at -1.00V. Potential linear sweep rates: *a*) 5 mV/s; *b*) 20 mV/s; *c*) 50 mV/s.

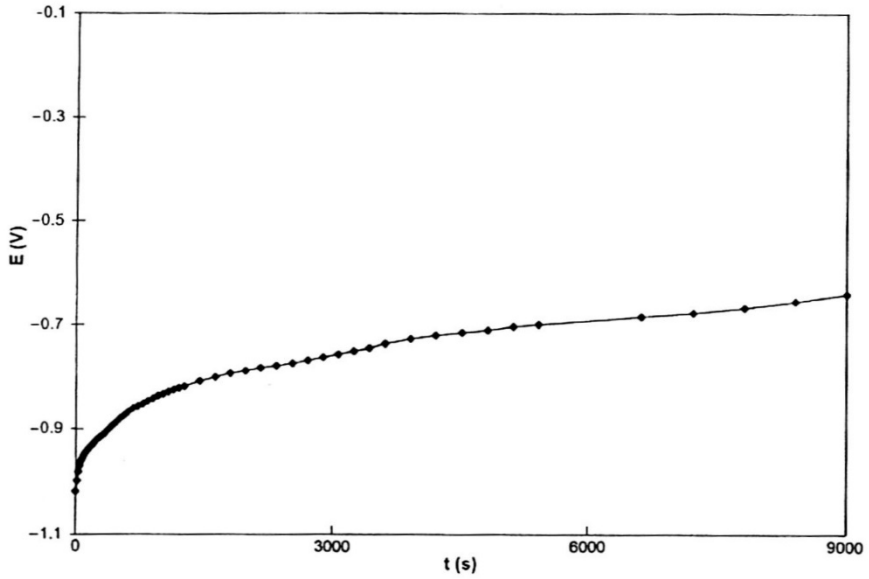

Figure 6. – Open-circuit potential decay of a sintered Ni electrode after ≈ 1 hour of potentiostatic electrolysis at -1.00 V (potentials are referred to s.c.e.).

Prolonging potentiostatic cathodic electrolysis from a few hours to more than one day had no significant effect on the amount of hydrogen thereafter extracted from Ni. However, the o.c. potential decay was seen to slow down appreciably with the duration of cathodic electrolysis, especially at 95°C, indicating that, although most of the hydriding reaction is restricted to near-surface layers, Ni hydride enclosures and/or thin plates deep in the metal structure are formed in time. This “deep” hydrogen is not easily driven to the surface by anodic stripping, owing to the low diffusion coefficient of hydrogen in Ni.

Some voltammetric runs were also performed in Na_2CO_3. The behavior shown in figs. 2-6 was substantially reproduced in most cases, but passivation of Ni was observed in a few experiments.

b) Electrode behavior of massive Ni. Massive Ni, without any surface treatment, was found to form no hydride phase. Instead, when massive Ni electrodes (sheet or rod) were etched for several days in diluted mineral acids and then submitted to anodic polarization, leading to surface blackening, subsequent cathodic polarization allowed the formation of β-hydride, identified by either voltammetric patterns or its o.c. potential.

TABLE I. — Electrochemical hydriding of sintered Ni in 0.6 M K_2CO_3. Area of electrode = 2.7 cm^2.

Run (no.)	Temperature (°C)	Reduction potential (V)	Duration of cathodic reduction (min)	Hydrogen extracted ([a])	
				(C)	(M)
1	25	-1.300	30	0.570	$0.30 \cdot 10^{-5}$
2	25	-1.350	1320	0.166	$0.09 \cdot 10^{-5}$
3	60	-1.300	15	1.30	$0.67 \cdot 10^{-5}$
4	60	-1.300	60	2.00	$1.04 \cdot 10^{-5}$
5	60	-1.300	100	3.00	$1.55 \cdot 10^{-5}$
6	60	-1.300	1080	2.40	$1.24 \cdot 10^{-5}$
7	95	-1.125	17	2.30	$1.19 \cdot 10^{-5}$
8	95	-1.150	60	3.00	$1.55 \cdot 10^{-5}$
9	95	-1.300	60	3.60	$1.87 \cdot 10^{-5}$
10	95	-1.300	120	8.50	$4.41 \cdot 10^{-5}$
11	95	-1.300	240	5.00	$2.59 \cdot 10^{-5}$

(*a*) Hydrogen extracted by anodic stripping at -0.8 V.

Compared with sintered Ni, the hydriding process was much less effective, as shown by the data reported in table II. It was also observed that the formation of Ni hydride was hindered by prolonging the cathodic polarization for more than a few minutes, which irreversibly degraded hydrogen absorption.

TABLE II. – Electrochemical hydriding of massive Ni in 0.6 M K_2CO_3. Area of electrode = 6.3 cm^2.

Run (no.)	Temperature (°C)	Reduction potential (V)	Duration of cathodic reduction (min)	Hydrogen extracted	
				(mC)	(M)
1	25	-1.200	< 1	70	$3.6 \cdot 10^{-7}$
2	25	-1.150	7	75	$3.9 \cdot 10^{-7}$
3	25	-1.150	15	92	$4.8 \cdot 10^{-7}$
4	60	-1.000	< 1	112	$5.8 \cdot 10^{-7}$
5	60	-1.050	7	147	$7.6 \cdot 10^{-7}$
6	60	-1.050	15	210	$10.9 \cdot 10^{-7}$
7	95	-1.050	3	193	$10.0 \cdot 10^{-7}$
8	95	-1.050	10	203	$10.5 \cdot 10^{-7}$
9	95	-1.025	15	163	$8.4 \cdot 10^{-7}$

3.2. Calorimetric results

The above electrochemical data show that the hydriding reaction resulting in the h.e.r. at Ni is

- much more extensive on sintered than on massive metal;
- strongly enhanced by temperature.

Therefore, assuming that Ni hydride formation is the physico-chemical condition for heat generation, sintered Ni was the preferred metal substrate, and electrolytic-calorimetric experiments were performed above room temperature, even close to the boiling point of the electrolyte.

Experimental design, procedure and results are illustrated in the following sections.

a) Non-isothermal calorimetry. Once the thermostat had been set above room temperature, the temperature attained by the electrolyte in the Dewar cell was still some degrees below that of the thermostating bath. Some heat was lost through the lid and cell sides not immersed in the bath, and other heat was lost by N_2 bubbling into the electrolyte, becoming greater at the highest temperature. However, it was verified that for a controlled N_2 flow (typically 50 bubbles/min), steady-state conditions were achieved between the heat input from the thermostat and the various losses, so that the electrolyte temperature was kept stable within ± 0.1°C. Thermal fluctuations of ± 1°C in the room temperature were reflected by ± 0.1°C in the electrolyte.

Electrolytic experiments and calorimetric measurements were preceded by calibration of the system. Once thermal equilibrium had been achieved, the cell constant (in °C/W) was determined by feeding the heater with a $V \cdot I$ known power and measuring the new equilibrium temperature achieved by the electrolyte. The cell constant allowed any temperature increase of the electrolyte to be converted into the equivalent heating power.

Electrolysis was carried out after calibration by applying a d.c. current between cathode and anode; the total power entering the cell was thus

i) $P_{\mathrm{E}}(\text{in W}) = I(\text{in A}) \cdot \mathrm{E}(\text{in V})$.

Of this power, 1.48(V) · (A) were spent for H_2O splitting in isothermal conditions, and the rest was dissipated as heat. The Joule power due to electrolysis is consequently given by

ii) $P_{\mathrm{J}} = I \cdot (E - 1.48)$.

In the absence of any anomalous heat effect, ΔT (temperature increase of the electrolyte) matches dissipated electrolytic power. In other words

iii) $\Delta T/k = P_{\mathrm{J}}(t)$

$P_J(t)$ accounts for the possible variation in Joule heating with electrolysis time.

Excess heating power, if any, is simply determined as

iv) $P_{ex} = \Delta T/k - P_J(t)$.

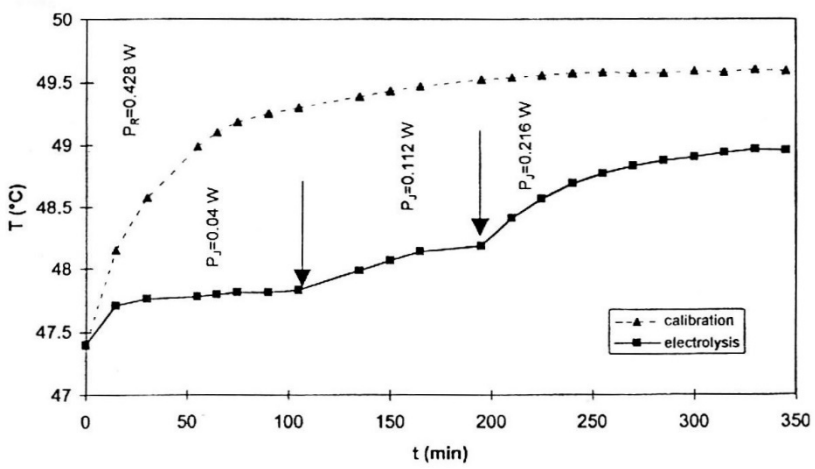

Figure 7. – Electrolyte temperature increase during calibration (dotted curve); electrolysis (plain curve). P_R: power to heater; P_J: electrolytic Joule power.

As a result of the above, an electrolytic-calorimetric experiment was carried out with the same sintered Ni sample ($2.1 \times 1.4 \times 0.06$ cm^3) and the same electrolytic solution (90 ml of 0.6 M K_2CO_3/H_2O) but at three different thermostatic bath temperatures. The electrolyte was periodically refilled to compensate for electrolytic consumption of H_2O.

In the first run, the thermostat was set at 50.00 ± 0.01°C; the equilibrium temperature attained by the electrolyte was 47.4 ± 0.1°C.

Before starting electrolysis, 0.428 W were fed to the heater, which caused a ΔT increment of 2.2 ± 0.1°C in the electrolyte temperature (k = 5.1°C/W): the dotted curve of fig. 7 illustrates this calibration. When the calibration power was switched off, the electrolyte relaxed to its initial temperature and the electrolysis current was applied. Figure 7 shows the temperature increase from the beginning of electrolysis (plain curve) and the Joule power (P_J) corresponding to the three currents applied. Comparison of calibration and electrolysis current reveals some heat in excess of Joule power. Quantitative data are reported in table III, which also illustrates later stages of the run. Excess power is given with an error σ accounted for by the ±0.1°C accuracy in temperatures measured both before and during electrolysis.

TABLE III. – σ = 0.04 W; k = 0.59 mA/W = 5.1°C/W.

I_e(A)	E(V)	P_J (W)	P_m(W)	P_{ex} (W)	P_{ex}/P_J(%)
0.1	1.883	0.040	0.097	0.057	142
0.2	2.066	0.117	0.165	0.048	41
0.3	2.260	0.234	0.315	0.081	35
0.3 (^{a})	2.250	0.116	0.203	0.087	75
0.35	2.350	0.305	0.404	0.099	32
0.4 (^{a})	2.474	0.199	0.285	0.086	43

(*a*) Pulsed current (3s on/3s off).

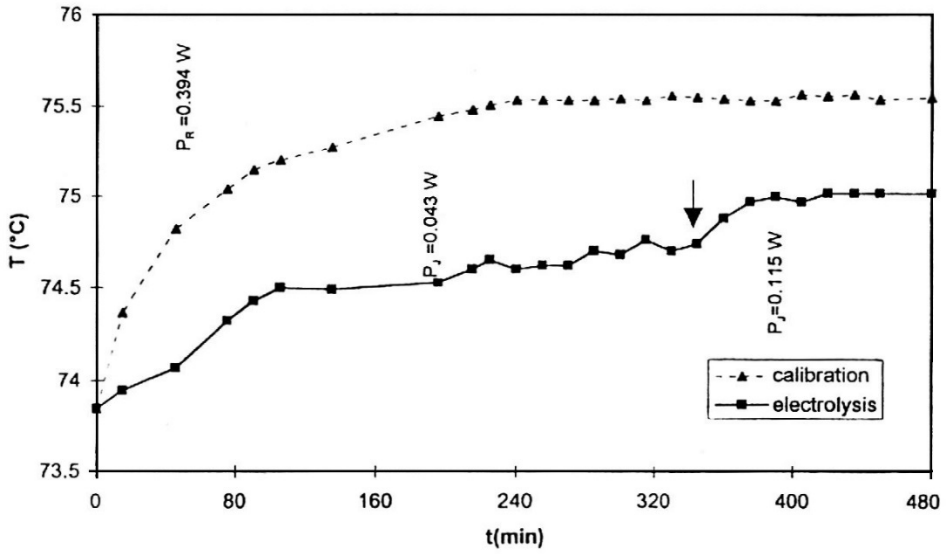

Figure 8. – Electrolyte temperature increase during calibration (dotted curve); electrolysis (plain curve).

The excess power data reported in table III are definitely above σ and appear to be self-consistent:

- ⇨ excess power increases with electrolysis current but, predictably, P_{ex}/P_J decreases;
- ⇨ the current matched with an asterisk was pulsed (3 s on, 3 s off): it is noted that the corresponding excess power was not below that measured in continuous d.c. feed.

In the second run the thermostat was set at 80.00 ± 0.01°C and the electrolyte equilibrium temperature was 73.8 ± 0.1°C. Calibration by one power step of 0.394 W (fig. 8, dotted curve) led to a cell constant of k = 3.8°C/W. Once the electrolyte had been reset to the initial temperature conditions, electrolysis was initiated at a current of 0.100 A and then led to 0.200 A:

the plain curve of fig. 8 accounts for the increase in electrolyte temperature. Excess heat appears more clearly than in the preceding run, as quantitatively shown by the data of table IV. Note that excess heat did not increase with current: this fact is provisionally ascribed to the heat loss caused by the electrolytic gas (see below). The thermal effects induced by pulsed current ((*a*) 3 s on/3 s off; (*b*) 10 s on/20 s off, see table IV) were greater than those obtained with d.c current.

TABLE IV. – σ = 0.045 W; k = 0.43 mA/W = 3.8°C/W.

I_e(A)	E(V)	P_J(W)	P_m(W)	P_{ex}(W)	P_{ex}/P_J(%)
0.1	1.908	0.043	0.228	0.185	430
0.2	2.053	0.115	0.320	0.205	178
0.25	2.085	0.151	0.334	0.183	121
0.15 (*a*)	2.111	0.047	0.300	0.253	538
0.15 (*b*)	2.112	0.032	0.313	0.281	878

(*a*) Pulsed current (3s on/3s off).
(*b*) Pulsed current (10s on/20 s off).

In the third run, the thermostat temperature was increased to 99.00 ± 0.01°C and the electrolyte temperature settled at 89.4 ± 0.1°C. Calibration was performed with an initial power step of 0.175 W subsequently increased to 0.302 W. This is marked by the dotted curve of fig. 9, which also shows the thermal relaxation of the electrolyte when, after 285 min, the heater power was turned off (cell constant k = 2.95°C/W). The plain curve of fig. 9 emphasizes both the remarkable temperature increase paralleling electrolysis (I = 0.150 A) and a quite unexpected phenomenon: after 240 min of electrolysis, in o.c. conditions, the electrolyte temperature did not decrease to its original value. In other words, the system showed a persistent thermal "after-effect": 0.300 W were still emitted by the electrode 4000 min after the cell had been taken to o.c.[*]

When the run was continued and electrolysis was restarted at 0.150 A, the electrolyte temperature again reached the levels shown in fig. 9. The data of table V show quantitative thermal effects at various stages of the run.

b) Isothermal calorimetry. In view of the considerable temperature effect on the thermal phenomenon, the subsequent steps of our investigation were carried out close to the electrolyte boiling point, in isothermal or quasi-isothermal conditions.

[*] Note added by Jed Rothwell: In most cold fusion papers this "after-effect" is called "heat after death," a term coined by Fleischmann and Pons.

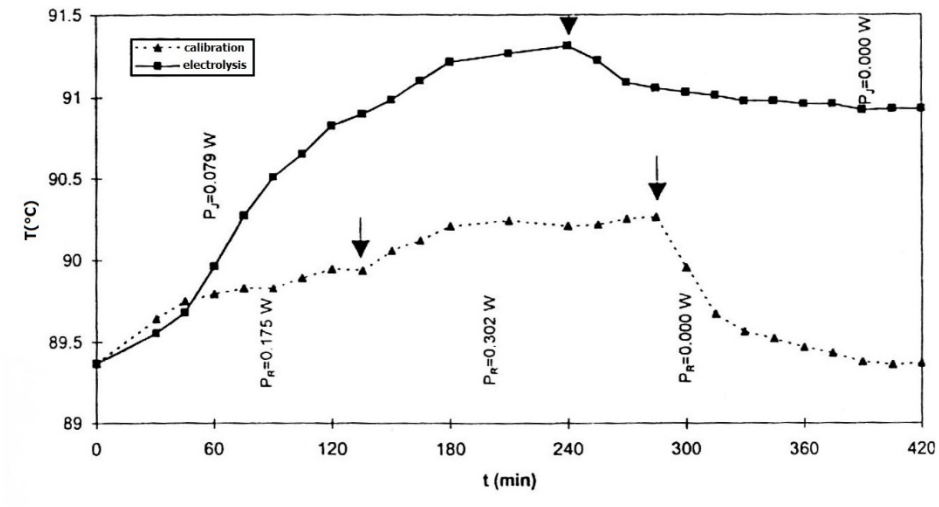

Figure 9. – Electrolyte temperature increments during calibration with three successive power steps (dotted curve) and electrolysis at 0.150 A, followed by o.c. conditions (plain curve).

TABLE V. – σ = 0.06 W; k = 0.334 mA/W = 2.95°C/W.

I_e(A)	E(V)	gas	P_J(W)	P_m(W)	P_{ex}(W)	P_{ex}/P_J(%)
0.15	2.005	N_2	0.079	0.66	0.581	734
o.c. after 30 min		N_2	0.000	0.58	0.583	—
o.c. after 930 min		N_2	0.000	0.44	0.440	—
o.c. after 2400 min		N_2	0.000	0.40	0.396	—
o.c. after 4000 min		N_2	0.000	0.386	0.386	—
0.15	2.021	N_2	0.081	0.668	0.587	725
o.c. after 1400 min		N_2	0.000	0.398	0.398	—

The thermostat was set at 95.0°C and the heater was continuously fed with the power (P_R^0) necessary to make the electrolyte isothermal with the outer oil bath. When a thermal event due to electrolysis or to something else occurred in the cell, the power to the heater was adjusted to balance this event. Excess power (see table V) at any time was consequently given by

v) $P_{ex}(t) = P_R^0 - P_R(t) - P_J(t)$,

where $P_R(t)$ is the power adjusted to maintain the electrolyte at 95.0 ± 0.1°C.

Electrolytic-calorimetric runs were preceded by tests with the blank cell, to assess the peculiarities of the adopted calorimetry.

The long-term stability of isothermal conditions (several days) was investigated first. It was found that, at constant P_R^0 input, the electrolyte settles at 95.0 ± 0.1°C, provided that there is no vapor leakage and that the N_2 flow into the cell is rigorously constant (thermal fluctuations of ±1°C in room temperature were reflected by ± 0.03°C in the electrolyte).

The need for good sealing is obvious: vapor loss means H_2O loss, with consequent positive drifts of cell temperature and cell constant. Although the original calorimetric conditions can be maintained by adding H_2O (in addition to that lost by electrolysis), vapor losses cannot easily be estimated.

As for the latter condition, with a gas flow rate in the range 2-3 ml/min, the heat loss due to gas thermal capacity is negligible (a few mW). However, at 95°C, N_2 flow gives rise to large evaporation and reflux of cold H_2O, both of which withdraw significant amounts of heat. Some blank tests were specifically designed to estimate heat loss correlated with gas flow. Thus, fig. 10 shows the drop in electrolyte temperature-induced by progressive increments of N_2 flow rate, while the power input to the heater (P_R^0) was kept constant. Likewise, fig. 11 shows how the calorimetric characteristics (k) of the blank cell filled with electrolyte degraded with N_2 flow rate.

The typical gas flow rate chosen for isothermal experiments was therefore in the range 50-62 bubbles/min (≈ 2.2-2.7 ml/min) which, once established, was periodically checked and adjusted to a tolerance not higher than ± 1 bubble/min. A flow rate in this range ensured that stirring was sufficient to maintain uniform temperature within the electrolyte without excessively degrading calorimetric sensitivity.

Temperature distribution within the electrolyte was investigated by either moving the thermometric probe from the bottom of the cell up to near the surface, or by equipping the blank cell with a second thermometer. Most points inside the cell were isothermal to within 0.1-0.2°C, provided they were not in close proximity to either heater or electrolyte surface: although cell heat sources (walls, heater) and heat sink (electrolyte surface) were both localized, no significant temperature gradient was established in the bulk electrolyte, at least for the chosen N_2 stirring rates. Electrolytic-calorimetric experiments were carried out with the Dewar cell having air in the interspace (favoring heat intake from the thermostat) and equipped with a lid thicker than in the blank cell (diminishing heat loss). This cell, charged with an amount of electrolyte (generally 90 ml) lower of that used in the blanks, had k values around 2°C/W. Also in the isothermal runs, the cell constant was always determined (before, during and at the end of electrolysis) to check calorimeter performance.

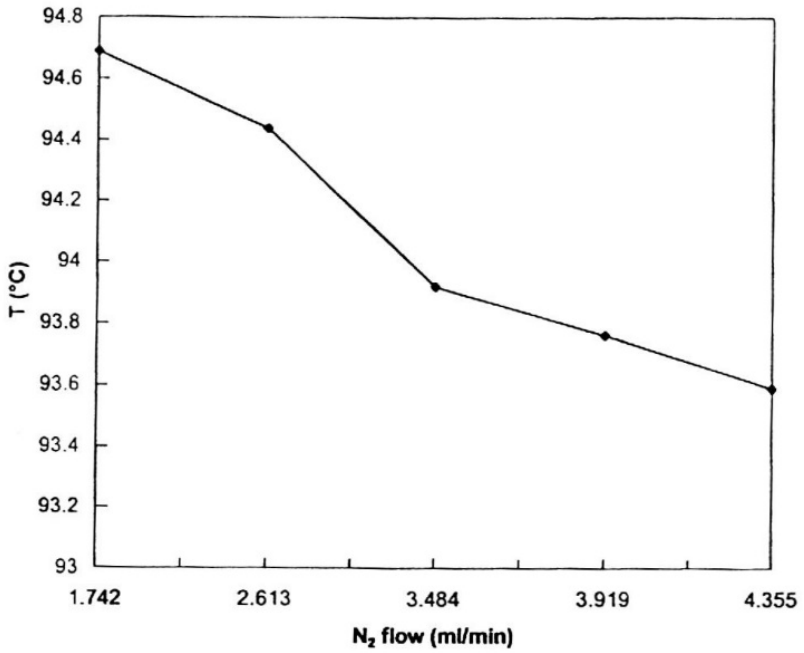

Figure 10. – Electrolyte temperature decrease with increasing N_2 flow rate. Thermostat temperature: 95.00°C.

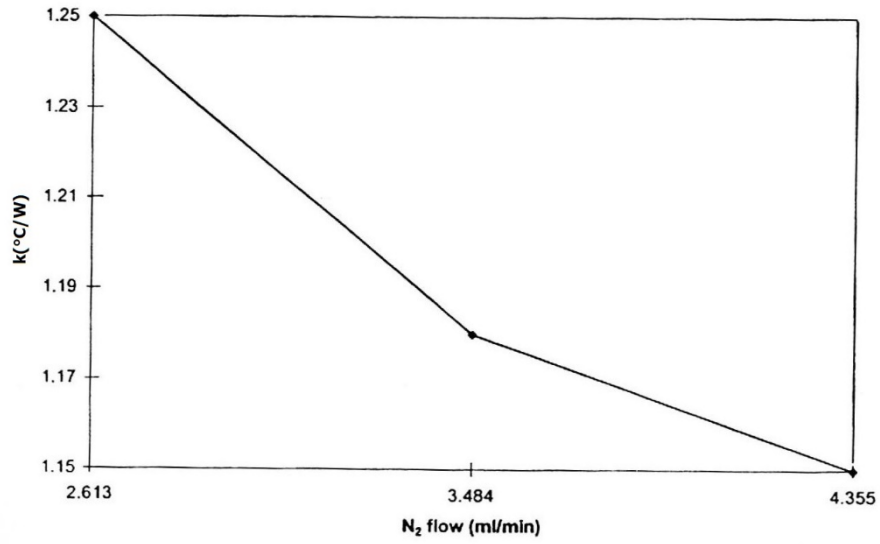

Figure 11. – Cell constant decrease with increasing N_2 flow rate. Thermostat temperature: 95.00°C.

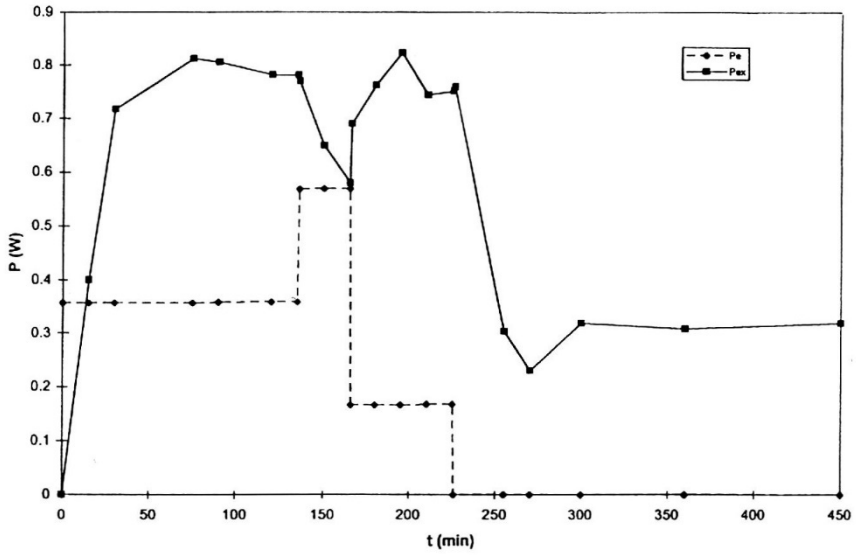

Figure 12. – Excess power (plain curve) measured in first isothermal experiment during 0.6 M K_2CO_3 electrolysis at sintered Ni. Dotted curve: total electric power entering cell.

Figure 12 shows the power measured in the first isothermal experiment. Electrolysis was initiated at 0.200 A, using a Ni cathode of dimensions 5.6 × 1.45 × 0.06 cm^3.

It is noted that:

i) excess heat production started *ab initio* very quickly, maximum heat output being reached within two hours;

ii) at 0.300 A, the phenomenon was comparable in extent to the total electric power ($I \cdot E$) entering the cell, but was twice the electric power at 0.200 A and nearly four times that at 0.100 A;

iii) the apparent power decrease observed at the highest current was due to greater heat loss caused by the electrolytic gas (see below);

iv) when the cell was taken to o.c., the electrolyte did not relax to its pre-electrolysis thermal state, due to a persistent “after-effect”.

The data of fig. 12 were substantially confirmed by the second isothermal experiment, carried out with an electrode of dimensions 5.0 × 1.6 × 0.06 cm^3 and a steady current of 0.200 A (see fig. 13). The extent of the thermal phenomenon is compared with both the total electric power and the Joule power input.

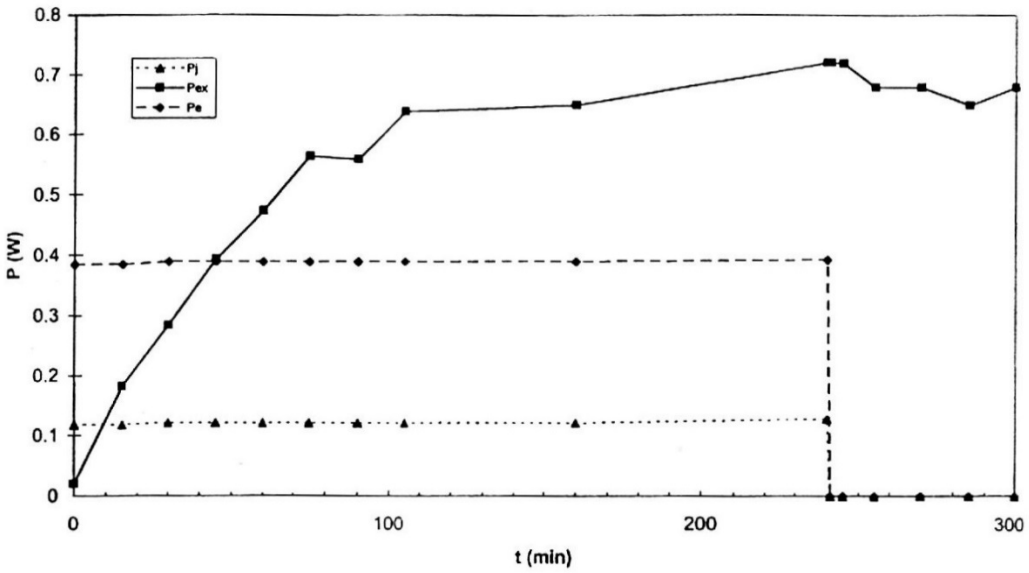

Figure 13. – Excess power (plain curve) measured during second isothermal experiment. Dotted curves: ● total electric power; ▲ Joule power input.

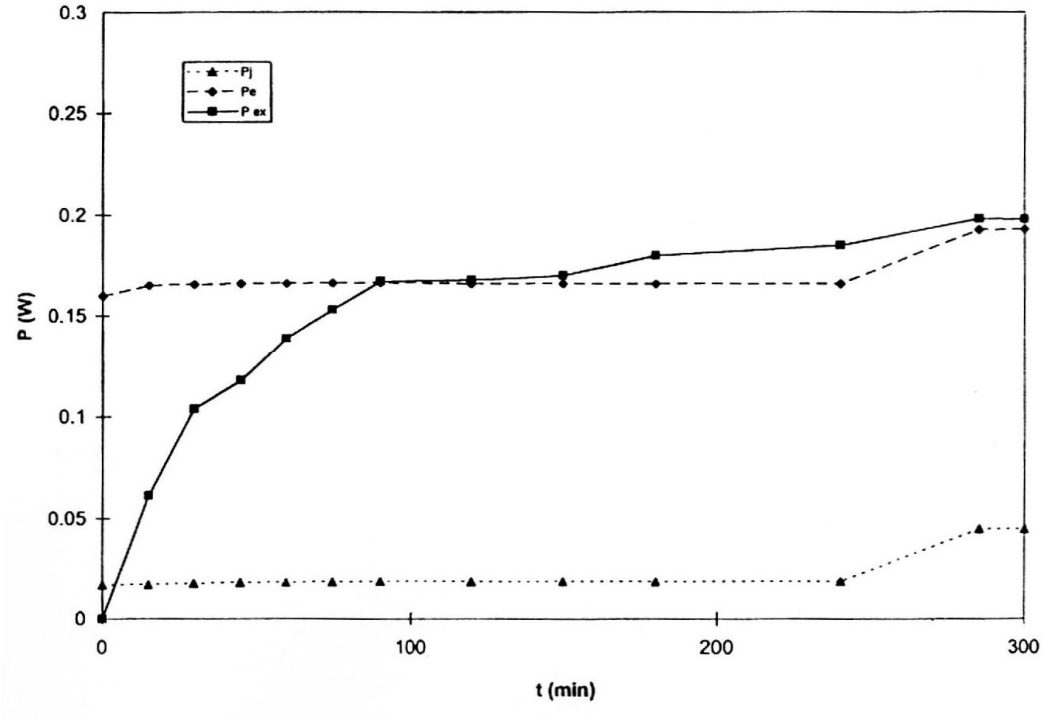

Figure 14.– Excess power (plain curve) measured by isothermal calorimetry during first 300 min of electrolysis of 0.6 M Na_2CO_3 at sintered Ni. Dotted curves: ● total electric power; ▲ Joule power input.

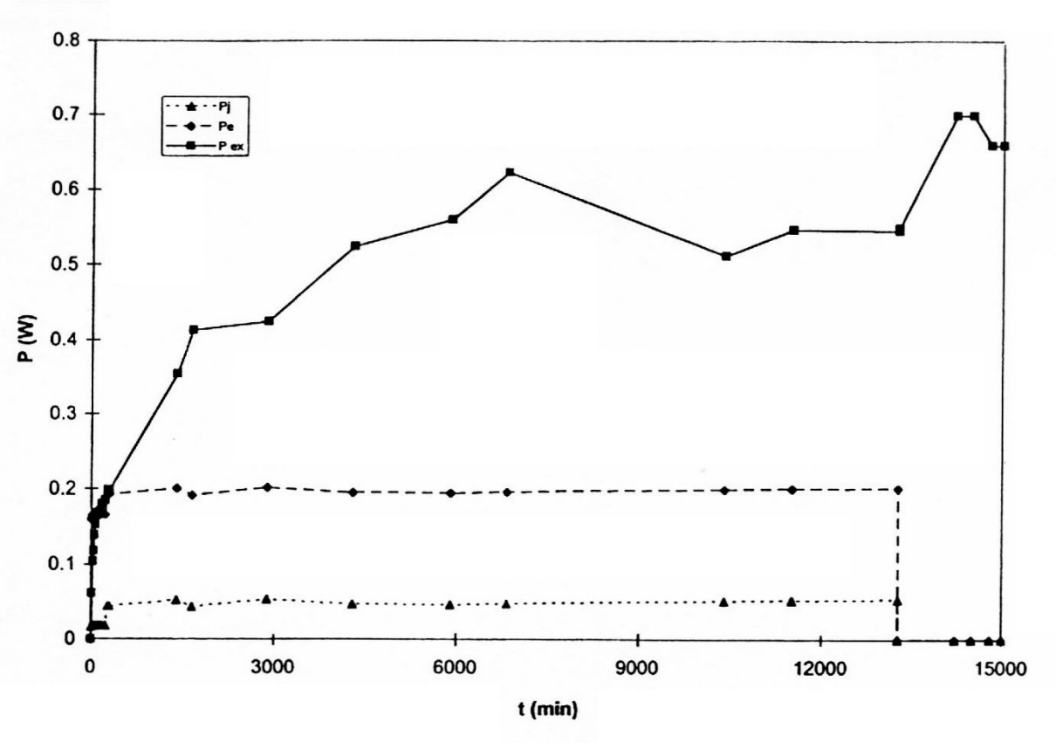

Figure 15. – Excess power (plain curve) measured by isothermal calorimetry during entire duration of the experiment in 0.6 M Na_2CO_3.

This second experiment was continued by alternating some more hours of electrolysis with a long rest in o.c., to observe how the heat produced without electrolysis decreased with time (very slowly).

The third isothermal experiment was carried out using 0.6 M Na_2CO_3 instead of K_2CO_3 as electrolyte. The dimensions of the Ni electrode ($4.6 \times 1.65 \times 0.06$ cm^3) were similar to those of the cathodes used in previous experiments and electrolysis was mainly performed at 0.100 A. Figure 14 shows the excess heat in the course of 5 hours of electrolysis. It may be seen that, although the initial rate of the thermal phenomenon was ≈ 75% slower than in K_2CO_3 (compare fig. 14 with figs. 12, 13), the heat output later progressively increased, as shown in fig. 15.

In other words, in these experiments, the main difference between sodium and potassium electrolytes only concerns the time scale on which the thermal phenomenon is established.

c) Reproducibility of the thermal phenomenon-Negative results. Seven other experiments were carried out at 95°C with K_2CO_3 electrolyte: of these, five gave excess heat comparable to that described above, and two gave negative results.

The first run was unsuccessful due to the presence in the electrolyte of a colored organic impurity which probably inhibited efficient hydride formation. This finding fits Mills' suggestion [2, 8, 9] that great care most be taken in order to avoid the presence of organic substances in the electrolyte.

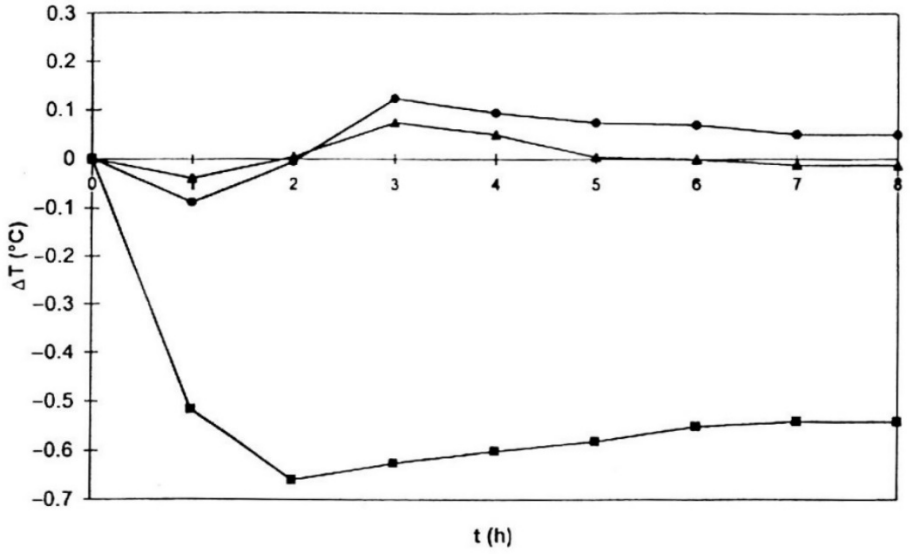

Figure 16. – Electrolyte temperature increments during 0.6M K_2CO_3 electrolysis at Ni electrodes pre-treated by: ● Pd plating; ▲surface oxidation with $K_2S_2O_7$; ■ dipping in concentrate HNO_3. Thermostat temperature: 95.00°C.

The second unsuccessful run involved a Ni sample which had been pre-oxidized by an O_2 stream bubbling for more than 24 hours in the electrolytic solution. This failure stresses the crucial importance of the state of the Ni surface for the induction of thermal effects. In order to investigate this matter in greater depth, before studying their electrolytic-calorimetric behavior, three Ni samples were submitted to different surface treatments: Pd electroless plating; surface oxidation in acidic $K_2S_2O_7$ solution; and dipping for one min in concentrate HNO_3. During electrolysis no excess heat was measured in any of the three cases as shown in fig. 16.

Note that surface pre-treatment in all positive runs involved the following steps:

i) rinsing with acetone to remove organic impurities,
ii) rinsing with H_2O,
iii) mild etching in 0.1 M HCl for 2-3 hours,
iv) rinsing with H_2O and storage in distilled H_2O.

4. – Discussion

This discussion focuses mainly on the conditions leading to the major thermal effect, *i.e.*, the results of the electrolytic-calorimetric runs carried out close to boiling point of the electrolyte.

The first point to be considered is the reliability of the calorimetric data. It has already been mentioned that thermometric measurements were made at a sensitivity level of ± 1 μA, so that estimated accuracy was ± 10 μA. In the isothermal runs, power was consequently measured at an accuracy of 40-60 mW, depending on both thermometric device and cell constant. In other words, the excess heat shown in figs. 13-15 ranged from ≈ 10 to ≈ 20 σ. However, since no

electrolytic blank system was specifically designed for comparison with those producing excess heat, it was possible that systematic errors affected the calorimetric data.

To verify this point, the following peculiarities of the adopted calorimetry must be recalled:

a) The system was stirred by a controlled stream of N_2 bubbles across the electrolyte, causing continuous withdrawal of heat.
b) The steady-state heat loss due to a N_2 flow rate in the range 2.2-2.7 ml/min (50-62 bubbles/min) amounted to several hundred mW (cfr figs. 10-11).
c) During electrolysis, additional gas was produced in the electrolyte at a flow rate ranging from 1.0 ml/min (0.100 A) to 3.0 ml/min (0.300 A), which further increased H_2O evaporation. As figs. 10, 11 show, the additional heat loss was at least some hundred mW or more, owing to the small size and high dispersion of the electrolytic gas bubbles.
d) The electric power necessary for electrolysis was quite low at 95°C owing to decreased electrolyte resistance, the corresponding Joule power was generally below 100 mW.

Therefore, since the heat loss due to gas developing at the electrodes was always larger than the Joule power input, the electrolyte was expected to cool down in the absence of anomalous heat sources. This is precisely what happened in the "negative" experiments (cfr. fig. 16) which thus constitute the blank tests and rule out the possibility of systematic errors. A corollary to this is that figs. 12, 13, 14 and 15 show excess heat which does not include the heat loss caused by the electrolytic gas, the real excess heat being some hundred of mW greater.

The second point to be considered is the extent of the thermal phenomenon. Both the low enthalpy release due to NiH_x formation [12] and the limited penetration of hydriding into the metal meant that the corresponding thermal effect is totally negligible. Instead, as figs. 12, 13, 15 and 16 show, excess heat may be many times greater than the total electric power entering the system, which rules out any conventional chemical or physico-chemical explanation of the phenomenon.

Excess heat measured in o.c. conditions (the "after-effect") and its very slow relaxation in time makes the matter still more intriguing.

The third point to be considered is the correlation between electrochemical hydriding of Ni and thermal effects. That Ni hydriding is the physico-chemical condition for excess heat induction is strongly supported by the parallel temperature effects observed in the extents of both hydriding (cfr. tables I, II) and excess heat (cfr. tables III-V). Since the "after-effect", was generally seen to increase with electrolysis time, it may provisionally be ascribed to hydride layers and/or hydrogen enclosures forming deep in the metal after prolonged cathodic polarization.

The nature of the thermal phenomenon is still very obscure. Mills' hypothesis is ruled out, at least for the catalytic cycle involving potassium, by the positive results achieved here with Na_2CO_3 electrolyte. Bush's hypothesis of "alkali-hydrogen fusion" is ruled out by the occurrence of substantial after-effects.

We may only state that the thermal phenomenon is caused by both surface and bulk processes, presumably induced by Ni hydriding.

REFERENCES

[1] PONS S., FLEISCHMANN M., WALLING C. and SIMONS J., *Method and Apparatus for Power Generation,* International application published under Patent Cooperation Treaty (PCT/US90/01328, International publication number WO 90/10935, Mar. 13, 1989).

[2] MILLS R. L. and KNEIZYS S. P., *Fusion Technol.,* **20** (1991) 65.

[3] NONINSKY V. C., *Fusion Technol.,* **21** (1992) 163.

[4] BUSH R. T., *Fusion Technol.,* **22** (1992) 306.

[5] RAMUZTHY H., SRINIVASAN M., MUKHERJEE V. K. and ADI BABU P., *Fourth International Conference on Cold Fusion, Maui, December 1993,* Abstract C.3.8; SANKARANARAYANAN T. K., SRINIVASAM M., BAJPAI M. B. and GUPTA D. S., ICCF-4 Abstract N2.4.

[6] NOTOYA R., *Fusion Technol.,* **24** (1993) 202.

[7] OHMORI T. and ENYO M., *Fusion Technol.,* **24** (1993) 293.

[8] MILLS R. L., GOOD W. R. and SHAUBACH R. M., *Fusion Technol.,* **25** (1994) 103.

[9] MILLS R. L. and GOOD W. R., *Fusion TechnoL,* **28** (1995) 1697.

[10] FOCARDI S., HABEL R. and PIANTELLI F., *Nuovo Cimento* A, **107** (1994) 163.

[11] SHKEDI Z., MCDONALD R. C., BREEN J. J., MAGUIRE S. J. and VERANTH J., *Fusion Technol.,* **28** (1995) 1720.

[12] BARANOWSKYI B., *Hydrogen in Metals II, Topics in Applied Physics,* Vol. **29**, edited by G. ALEFELD and J. VOÖL, (Springer, Berlin) 1978, p. 173.